Int J Adv Manuf Technol (2016) 87:3337–3348
DOI 10.1007/s00170-016-8710-5

ORIGINAL ARTICLE

Sensorless cutting force estimation for full-closed controlled ball-screw-driven stage

Yuki Yamada[1] · **Yasuhiro Kakinuma**[1]

Received: 19 June 2015 / Accepted: 4 April 2016 / Published online: 13 April 2016

Abstract Process monitoring technology has been studied in order to realize higher efficiencies and greater automation of the machining process. The cutting force is widely regarded as being the most valuable physical quantity to be gathered when monitoring a metal-cutting process. However, a practical, wideband, and indirect means of measuring the cutting force has not yet been attained for ball-screw-driven machine tools. In recent years, full-closed ball-screw-driven stages mounting linear encoder have been widely used for high-end machine tools. Considering indirect cutting force estimation using servo information from a full-closed controlled ball-screw-driven stage, three pieces of information are available as servo signals of the feed drive: the motor current command, the rotation angle of the motor, and the displacement of the stage. In this study, a high-precision and wideband sensorless cutting force estimation method was proposed for full-closed controlled ball-screw-driven stages using a multi-encoder-based disturbance observer (MEDOB). The MEDOB was originally proposed for estimating the external force on the load side of flexible robots, and was used for resonance ratio control, which was intended to suppress low-frequency vibration. This study aimed to develop an estimation technique for high-frequency cutting forces that exceed the bandwidth of current control loops for the highly stiff ball-screw-driven stage. The influence of extra phase lag on the control signals was considered in order to apply MEDOB to an actual ball-screw-driven stage. The validity of the proposed method was verified using both an analytical simulation and cutting experiments.

✉ Yuki Yamada
yamada@ams.sd.keio.ac.jp

[1] Department of System Design Engineering, Keio University, 3-14-1 Hiyoshi, Kohoku-ku, Yokohama 223-8522, Japan

Keywords Process monitoring · Ball-screw-driven stage · Cutting force · Disturbance observer · Multi-encoder-based disturbance observer

1 Introduction

With the ongoing development of CNC machine tools, a need has arisen for an effective scheme for monitoring the cutting process [1, 2]. In particular, the cutting force is directly related to the dynamics of the cutting process; hence, monitoring of the cutting force would provide a means of investigating the process behavior and detecting abnormal states, such as tool wear or tool breakage [3–5]. In addition, chatter has long been one of the major problems in the field of machining [6–8]. While tool wear can be detected by monitoring the mean component of the cutting forces, chatter often occurs near the resonance point at higher frequencies. Therefore, wideband cutting force measurement techniques are required to detect the entire unknown abnormal state. In general, cutting forces are measured using a dynamometer. However, dynamometers greatly increase initial costs and decrease loop stiffness from the tool to the workpiece. Thus, numerous previous studies of indirect cutting force measuring techniques have been done.

In the sensor-based techniques, displacement sensors such as capacitive [9], inductive [10] and eddy-current type [11] are often attached to a spindle, and cutting force is estimated by position variation induced by cutting force. Although the use of additional displacement sensors improves the accuracy of the cutting force estimation, a decrease in reliability is inevitable, and the reduction in maintainability is noteworthy when sensors are embedded inside the spindle. Calibration of the thermal influence and of the spindle stiffness is also required. On the other hand, cutting force measurement using internal sensors has also been the subject of studies. Monitoring the armature current of the feed drive or of the spindle motor is a typical example [12–15]. Altintas et al. [12]

established a cutting force monitoring methodology for a DC servo motor, and Lee et al. [13] extended to an AC servo drive. Kim et al. [14] estimated the cross-feed directional cutting force which is normal to machined surfaces, and estimation bandwidth was expanded to 130 Hz. Sato et al. [15] extracted cutting force components included in motor torque of feed drive by time-frequency analysis. Although the monitoring of the armature current is practical, the measurement bandwidth is narrow. This happens because the dynamics of the movable mass are not directly considered. Cutting force measurement based on the disturbance observer (DOB) theory [16] was proposed as a means of taking the dynamics of the moving mass into account [17–19]. Shinno et al. [17] showed that the cutting force can be estimated independent of temperature, in contrast to measurements with a dynamometer. Ibaraki et al. [18] proposed a method of estimating the cutting force by geometrically combining the cutting force vectors acquired from the feed drive and the spindle. Takei et al. [19] showed that estimation bandwidth can be expanded by using multi-rate sampling in the linear motor-driven stage. Although current signals cannot follow cutting force variations, which have higher frequency components, enhanced responsiveness (through consideration of the dynamics of the movable mass) and wideband estimation were accomplished.

Cutting force estimation with DOB is effective for linear motor-driven stages; however, accurate cutting force estimation has not been achievable in the case of ball-screw-driven stages. Since a ball-screw-driven system is composed of many mechanical elements, which transform rotational motion to translational motion, there are multiple resonance points. In addition, the friction forces between the nut, balls, and lead screw are large and are position- and angle-dependent. Furthermore, the nonlinear spring characteristic between the screw and the nut makes estimation of the even more difficult. These factors limit both estimation accuracy and bandwidth.

In recent years, full-closed ball-screw-driven stages mounting linear encoder have been widely used for high-end machine tools. Considering indirect cutting force estimation using servo information from a full-closed controlled ball-screw-driven stage, three pieces of information are available as servo signals of the feed drive: the motor current command, the rotation angle of the motor, and the displacement of the stage. However, the conventional DOB-based cutting force estimation method was intended for semi-closed control systems, and only a few studies have been conducted on in-process cutting force measurement methods integrating the three aforementioned signals. In this paper, a high-precision and wideband sensorless cutting force estimation method was proposed for full-closed controlled ball-screw-driven stages applying a multi-encoder-based disturbance observer (MEDOB) [20]. The MEDOB was originally proposed for estimating the external force on the load side of flexible robots and used for resonance ratio control [21], which aimed to suppress low-frequency vibration and to enhance control bandwidth. The concept of the MEDOB is applicable as a cutting force estimation method in a full-closed controlled ball-screw-driven stage when used with two encoders. However, this method is not directly adopted without any modification, because there are several sources of error in actual ball-screw-driven machine tools. Lag elements in the control system are non-negligible when estimating cutting forces at higher frequencies. In addition, unnecessary vibration excited by the motor current reference negatively influenced the estimation. In this paper, a methodology is presented for introducing wideband cutting force estimation with MEDOB, which includes phase compensation, to an actual full-closed controlled ball-screw-driven stage. Considering the influence of the lag elements and the vibration sources, it is shown that the MEDOB performed effectively as a wideband cutting force estimation method. Ultimately, the estimation method is applicable to the detection, avoidance, and suppression of tool wear, breakage, and chatter.

Nomenclature

a_t	Acceleration of table [m/s^2]
C_t	Viscous friction coefficient of translational element [N · s/m]
D_r	Viscous friction coefficient of rotational element [N · m · s/rad]
F_{cut}	Cutting force [N]
F_{fric}	Friction force [N]
F_l	Load force [N]
g_{cut}	Cutoff frequency of low-pass filter [rad/s]
l_a	Motor current [A]
l_a^{comp}	Compensation current for disturbance force [A]
J_r	Total inertia of motor, coupling, and ball-screw [kg · m^2]
K_r	Total rigidity of feed screw system [N/μm]
K_t	Torque coefficient [N · m/A]
ℓ	Lead [mm]
M_t	Movable mass [kg]
R	Transform coefficient for rotational motion to translational motion (= $\ell/2\pi$) [mm/rad]
T_m	Motor torque [N · m]
T_{fric}	Friction torque [N · m]
T_1, T_2	Identified dead time [s]
T_a, T_b, T_c	Dead time for phase lag compensation [s]
v_t	Velocity of table [m/s]
x_t	Displacement of table [m]
α_m	Angular acceleration of motor [rad/s^2]
θ_m	Angle of motor [rad]
ω_{ele}	Electrical delay of motor [rad/s]
ω_m	Angular velocity of motor [rad/s]
ω_{comp}	Cutoff frequency of compensation filter [rad/s]
Caret	Estimated value
$(\text{Subscript})_n$	Nominal value
$(\text{Superscript})^{cmd}$	Command value
$(\text{Superscript})^{ref}$	Reference value
$(\text{Superscript})^{res}$	Response value

2 Methodology

2.1 Modeling of ball-screw-driven stage [22]

The structure of a typical ball-screw-driven stage is shown in Fig. 1. The ball screw is connected, via a coupling, to a servomotor. This assembly drives the table carrying the workpiece by transforming the rotary motion of the motor into linear motion. In this study, a dual-inertia model was applied to describe the dynamic behavior of the ball-screw-driven stage. The model is shown in Fig. 2a. The dynamic equations are as follows:

$$J_r\alpha_m = T_m - T_{fric} - D_r\omega_m - K_r(R\theta_m - x_t)R \tag{1}$$

$$M_t a_t = K_r(R\theta_m - x_t) - C_t v_t - F_l \tag{2}$$

A block diagram of the dual-inertia system is shown in Fig. 2b. When the bandwidth of the current loop was high enough, the current reference, I_a^{ref}, and response current, I_a^{res}, were regarded as equivalent. The motor torque, T_m, and load force, F_l, in Eqs. (1) and (2) were rewritten as follows:

$$T_m = K_t I_a^{ref} \tag{3}$$

$$F_l = F_{cut} + F_{fric} \tag{4}$$

To make the frequency analysis simpler, Eqs. (1) and (2) were rearranged in the Laplace domain, as follows:

$$\begin{bmatrix} \theta_m \\ x_t \end{bmatrix} = \frac{1}{M_t J_r E(s)} \begin{bmatrix} M_t s^2 + C_t s + K_r & RK_r \\ RK_r & J_r s^2 + D_r s + R^2 K_r \end{bmatrix} \begin{bmatrix} T_m \\ -F_l \end{bmatrix} \tag{5}$$

where

$$\mathrm{E(s)} = s^4 + 2(\alpha\zeta_r + \zeta_t)\omega_t s^3 + (4\alpha\zeta_t\zeta_r + \alpha + 1)\omega_t^2 s^2 + 2\alpha(\zeta_r + \zeta_t)\omega_t^3 s$$

$$\omega_t = \sqrt{\frac{K_r}{M_t}},\ \zeta_r = \frac{D_r}{2\omega_t M_t R^2},\ \zeta_t = \frac{C_t}{2\omega_t M_t},\ \alpha = \frac{M_t R^2}{J_{rn}}$$

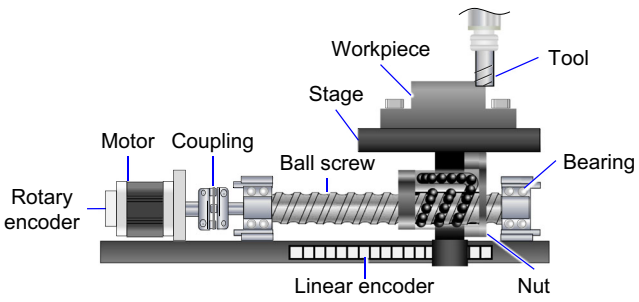

Fig. 1 Typical structure of ball-screw-driven stage

2.2 Cutting force estimation method using MEDOB based on dual-inertia model

In the conventional DOB-based method, the equation to estimate cutting force was introduced based on a single-inertia (i.e., rigid body) model of the ball-screw-driven stage [23]. However, estimation bandwidth is limited owing to the natural modes, because dynamic behavior between translational and rotational elements was not considered. For higher precision and a wider band, a cutting force estimation method considering the mechanical dynamics (i.e., expansion to a multi-inertia system) needed to be presented. By making use of the characteristics of the full-closed controlled system, the DOB was expanded for application to a dual-inertia system by using the MEDOB. The estimation principle will be introduced in this section.

Based on the dual-inertia model, the cutting force, F_{cut}, was obtained by combining Eqs. (1), (2), (3), and (4), so that the reaction force, $K_r(R\theta_m - x_t)$, could be erased. The cutting force, F_{cut}, was expressed as follows:

$$F_{cut} = \frac{1}{R}\left(K_t I_a^{ref} - J_r\alpha_m - D_r\omega_m - T_{fric}\right) - M_t a_t - C_t v_t - F_{fric} \tag{6}$$

When cutting force is calculated from Eqs. (2) and (4), the stiffness, K_r needs to be used, which varies depending on the displacement of the stage. On the other hand, the cutting force is expressed without using the stiffness, K_r, in Eq. (6). Thus, identification of stiffness is not required in the cutting force calculation based on the dual-inertia model. An equation for estimating the cutting force was introduced, as follows:

$$\hat{F}_{cut} = \frac{g_{cut}}{s + g_{cut}}\left\{\frac{1}{R}\left(K_{tn} I_a^{ref} - J_{rn}\alpha_m - D_{rn}\omega_m - \hat{T}_{fric}\right) - M_{tn} a_t - C_{tn} v_t - \hat{F}_{fric}\right\} \tag{7}$$

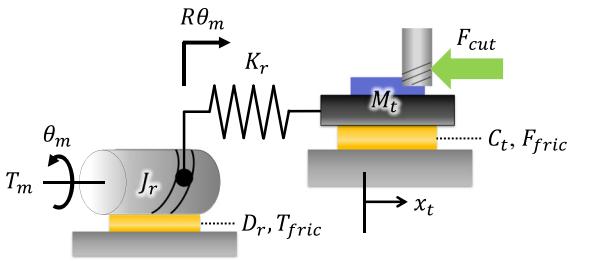

(a) Model of dual-inertia system

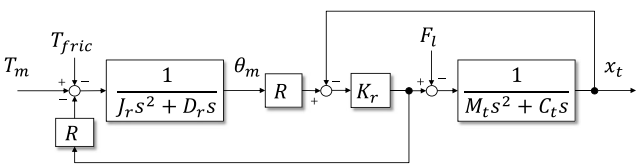

(b) Block diagram of dual-inertia system

Fig. 2 Model of ball-screw-driven stage

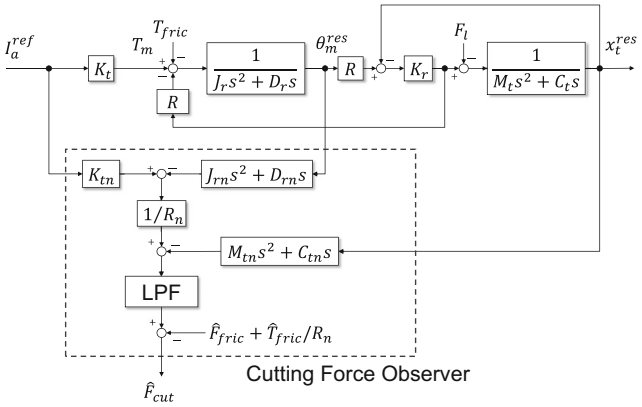

Fig. 3 Block diagram of cutting force observer based on MEDOB

A first-order low-pass filter was implemented to eliminate higher-frequency noise, which arises when differentiating the position signal to calculate the acceleration or velocity signal. Since I_a^{ref}, θ_m, and x_t are available as servo signals in the full-closed controlled ball-screw-driven stage, the cutting force can be estimated with adequate identification of the friction torque, T_{fric}, and the friction force, F_{fric}. Based on Eq. (7), block diagram of the cutting force observer was introduced as shown in Fig. 3. In this study, the rectangular portion surrounded by the dashed line is called the cutting force observer.

As described above, cutting force was estimated on the basis of feed drive model, which means cutting mechanics is unnecessary. On the other hand, the proposed method has a possibility to incorporate cutting mechanics. For example, cutting force would be theoretically predictable under stable cutting condition by using an instantaneous cutting force model if cutting force constant [24] was known in advance. In that case, it is possible to compare the estimated cutting force by the observer with the predicted one from the cutting mechanics model and to detect tool wear from the comparison.

3 Simulation

Numerical simulations were conducted to demonstrate how the estimation accuracy was influenced by the motion of each mass in dual-inertia model. In the simulations, sinusoidal load forces that had no DC components were applied for each frequency. The amplitude of the load force, F_l, was set to 10 N. To evaluate the estimation accuracy of both the DOB and the MEDOB, we calculated the ratio of the amplitude of the applied force to the estimated force. The ratio for each method was compared by increasing frequencies of the sinusoidal load forces. In the cutting force observer, a second-order low-pass filter, $\{g_{cut}/(s+g_{cut})\}^2$ was used as the LPF denoted in Fig. 3. The parameters used in this simulation are listed in Table 1. Parameters were set so that the resonant frequency of the driven system came close to 400 Hz. In order to focus on evaluating the estimation characteristics under ideal conditions, several sources of error in the estimation were not considered, such as friction forces, resolution of position signals, phase lag elements, and parameter identification errors.

Figure 4 illustrates the frequency characteristics of each estimated cutting force. Independent of whether the DOB or the MEDOB were used, the amplitudes of the estimated forces were nearly equal to those of the applied forces at frequencies from 10 to 50 Hz. However, both the amplitude and the phase vary widely and rapidly around the resonant frequency when the DOB was adopted as the estimation method. With the use of the MEDOB, the estimated results follow the second-order low-pass filter, $\{g_{cut}/(s+g_{cut})\}^2$, from 10 to 1000 Hz, including the resonant frequency. Therefore, we found that the estimation bandwidth expanded considerably as a result of applying the MEDOB under ideal conditions. The estimation method itself needs to be expanded for a multi-inertia model when the control object is modeled as a multi-inertia system. Estimation performance was substantially improved by making use of all control signals available in the full-closed controlled system, which was impossible with the use of the conventional DOB in a semi-closed control system.

4 Experimental setup

4.1 Experimental setup and control system configuration

To demonstrate the validity of the proposed method, several experiments to measure the cutting force were performed with

Table 1 Simulation parameters

J_r	Total inertia of motor, coupling, and ball screw [kg · m^2]	3.7×10^{-5}
M_t	Total movable mass [kg]	7.0
C_t	Viscous friction coefficient of translational element [N · s/m]	5.5×10^3
D_r	Viscous friction coefficient of rotational element [N · m · s/rad]	3.7×10^{-3}
K_r	Total rigidity of feed screw system [N/μm]	42.5
ℓ	Lead [mm]	5.0
T_s	Sampling time [μs]	20
K_t	Motor torque coefficient [N · m/A]	0.2
g_{cut}	Cutoff frequency of cutting force observer [rad/s]	4000

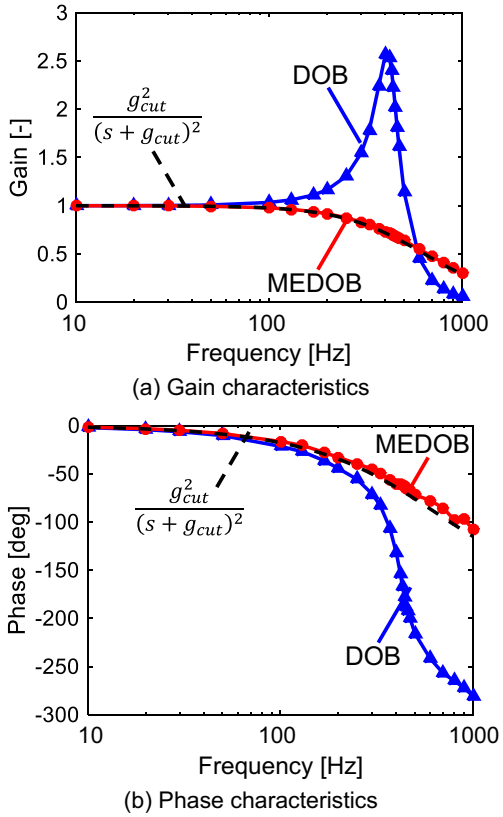

Fig. 4 Frequency characteristics of cutting force estimation

a single-axis ball-screw-driven stage. A schematic diagram of the experimental setup is shown in Fig. 5. The system consisted of a synchronous AC servomotor, a coupling, a ball screw (lead length 5 mm), two linear ball guides, and a dynamometer. The motor angle, θ_m, was obtained from the rotary encoder (resolution 17 bit) built into the motor (NA80-20, from Nikki Denso). The table displacement, x_t, was measured using a linear encoder attached to the table (LIF471R, resolution 20 nm, from HEIDENHAIN). The motor angle and the table displacement were fed back to the controller through the counter board. The controller generated a current reference from this feedback data, and the control program ran under the RT-AI real-time operating system. The bandwidth of the motor's current control loop was designed to be 4000 rad/s. A dynamometer (Type 9129A, from Kistler) was mounted on the table to accurately measure the cutting forces.

4.2 Friction compensation

To estimate the cutting force using Eq. (7), the friction torque, $\hat{T}_{fric}$, and friction force, $\hat{F}_{fric}$, must be accurately identified, because the identification accuracy of the friction force greatly affects the estimation accuracy of the cutting force. In this research, the friction torque and force were determined by performing an idling test. The output of the cutting force observer in Eq. (7) must be zero when a cutting force is not applied. Thus, the summation of the friction torque and friction force can be identified by moving the ball-screw-driven stage at a constant feed rate for eliminating the inertial force. Figure 6 shows an example of the friction characteristics identified through a single experiment. As shown in this figure, the estimated friction force varied depending on the position of the stage. In addition, the friction force fluctuated at a low frequency with a period of 5 mm. The amplitude of these fluctuations was about 10 N, for which compensation had to be applied to enable accurate estimation. On the other hand, it was confirmed that the summation of the friction force and friction torque had repeatability. The first and second results from the idling test were lower than the other results. Position-dependent friction force is almost similar after third idling test as shown in Fig. 7. Although friction force was high, standard variation was less than 10 N. For example, standard deviations for third-fifth results with respect to mean value of third-fifth results were 4.32, 3.85, and 4.14 N, respectively. The per-5-mm fluctuations were observed for a range of feed rates as

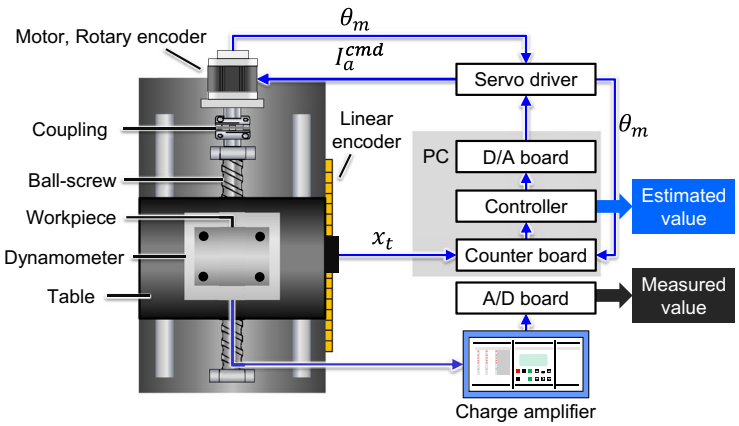

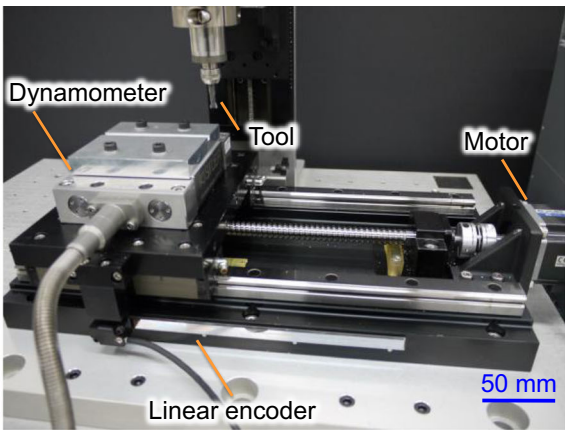

Fig. 5 Experimental setup

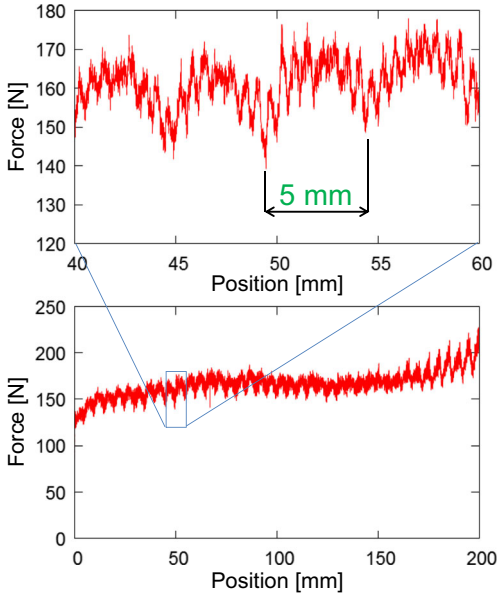

Fig. 6 Friction characteristics (feed rate 1 mm/s)

shown in Fig. 8, which suggests that the fluctuations are repeatable but cannot be ignored for high-precision monitoring. Thus, in this research, friction forces were compensated by idling tests. The idling test was conducted five times before the cutting test was performed. Then, the first and second results from the idling test were discarded and the remaining three results were averaged to ensure accuracy. From this step, the total friction force, $\hat{T}_{fric}/R + \hat{F}_{fric}$ was identified. Only if the total friction force has repeatability, friction compensation by idling test is applicable for attenuating friction fluctuations. In order to exploit position-dependency, position trajectory and velocity in the idling test and those in the cutting tests

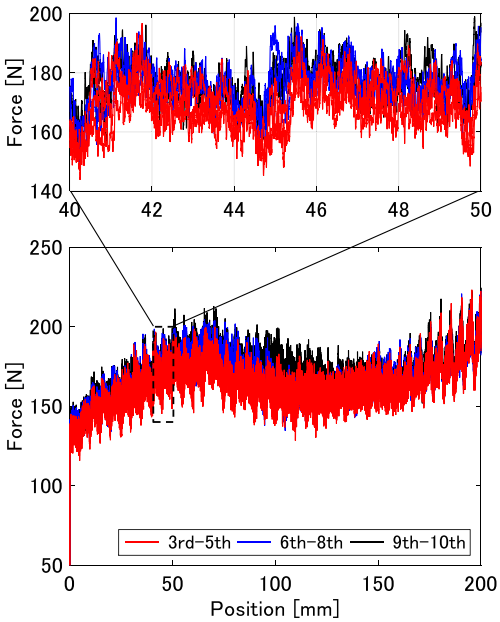

Fig. 7 Repeatability of friction force (feed rate 5 mm/s)

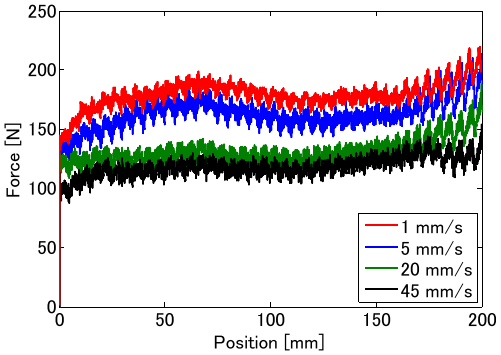

Fig. 8 Friction characteristics for different feed rates (test conducted 10 times; *lines* shown are averages)

need to be correspondent as much as possible. The end milling tests showed that cutting force which was sufficiently smaller than friction force could be monitored as long as position dependency of friction force was sufficiently high.

Many researchers have investigated the friction characteristics of ball-screw-driven systems, especially at a microscopic level [25–27]. In addition to the idling test, implementation of these methods on a microscopic level could improve compensation accuracy. In future work, we plan to integrate these methods with the idling test for highly accurate friction compensation.

5 Experiment

5.1 Experimental conditions for cutting force monitoring test

A milling test was performed to verify the validity of the cutting force observer, based on the MEDOB. The single-axis ball-screw-driven stage in which the cutting force observer was installed is shown in Fig. 5. The cutting tool was rotated by a brushless spindle motor (EMS-3056, from Nakanishi) installed vertically. A table-type dynamometer (Type 9129A, from Kistler), attached between the table and workpiece, was

Table 2 Experimental conditions

Spindle speed [min^{-1}]	1000–12,000
Cutoff frequency of low-pass filter [Hz]	400
Type of low-pass filter	Butterworth (8th order)
Cutting tool	Square end mill (ϕ 6.0 mm, 2 flute)
Helical angle [deg]	30
Workpiece material	Al alloy (A5052)
Immersion type	Full immersion
Axial depth of cut [μm]	180
Feed per tooth [μm /tooth]	30
Sampling time [μs]	50
Control interval [μs]	200

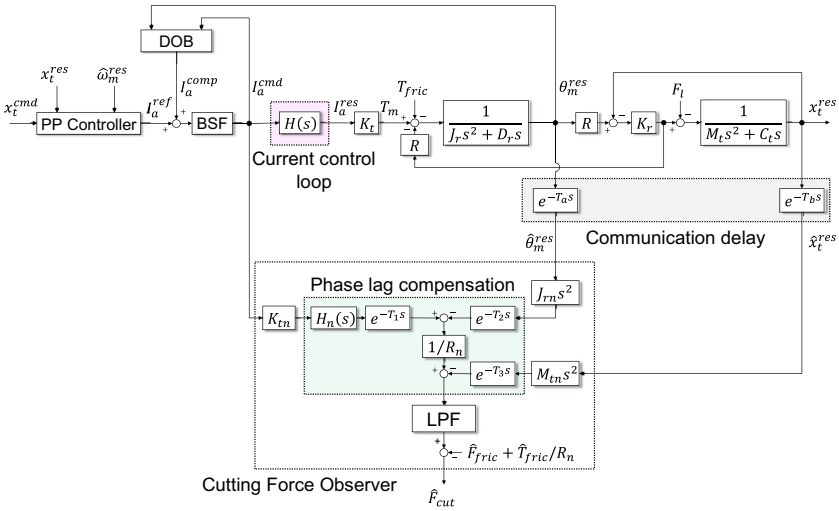

Fig. 9 Block diagram of cutting force estimation system with phase lag compensation

used for measuring the actual cutting force. In the cutting test, the spindle speeds were varied between 1000 min^{-1} and 12, 000 min^{-1} in order to evaluate the estimation accuracy as a function of the frequency of the applied cutting forces. Slots were machined without any lubricant, and feed rate was kept constant during cutting. The parameters applied to the cutting test are listed in Table 2. A tiny axial depth of cut was applied in order to show that smaller cutting force was observable. The cutoff frequency of the low-pass filter was set to 400 Hz so that the dominant resonant frequency was included within the pass-band. In addition, the low-pass filter was changed to a Butterworth type (8th order) to enhance the noise-cancelation ability. Note that not only the estimated cutting force, but also the force measured by the dynamometer, were filtered for fair comparison. The total friction force was identified according to the procedure in Section 4.2. Because friction compensation was conducted by idling test at the same velocity as cutting test, the damping force excluding the component of the velocity variation due to cutting force is included in the compensated friction force. Thus, DC component of the estimated velocity was almost diminished. In addition, velocity variation induced by cutting force was sufficiently suppressed owing to servo control. Thus, viscous coefficients, C_t, and D_r, were not considered in the cutting force observer. Mechanical parameters were identified experimentally by swept sine excitation, and specific values will be shown in the next section.

5.2 Identification and compensation of phase lag

As mentioned in chapter 3, wideband cutting force estimation was feasible with the use of the MEDOB under ideal conditions. However, the original MEDOB was not directly applicable for the actual equipment because of synchronization errors between control signals. When estimating high-frequency cutting forces, the effects of the phase lag elements are non-negligible.

Figure 9 shows the cutting force observer with a phase lag compensation function. Position control was performed by the combination of the conventional position-P velocity-P controller and the DOB. Before generating a current command, I_a^{cmd}, a band-stop filter (BSF) was applied to the summation of the motor current reference, I_a^{ref}, and the compensation

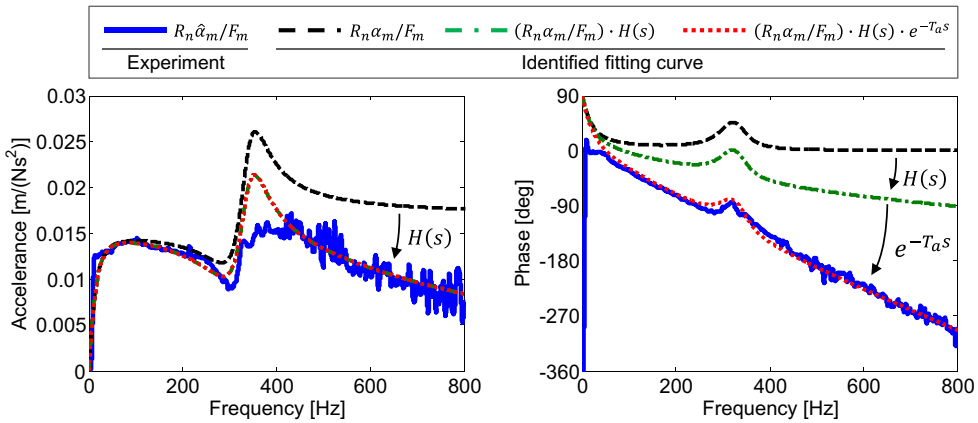

(a) Gain characteristics (green dotted-dashed line overlaps with red dotted line)

(b) Phase characteristics

Fig. 10 Frequency response functions of $R_n\alpha_m/F_m$ and $R_n\hat{\alpha}_m/F_m$

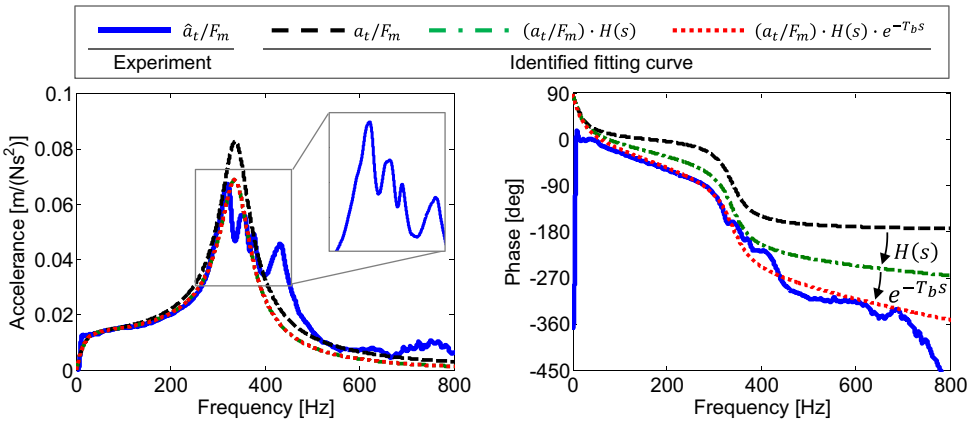

(a) Gain characteristics (green dotted-dashed line overlaps with red dotted line)

(b) Phase characteristics

Fig. 11 Frequency response functions of a_t/F_m and $\hat{a}_t/F_m$

current, I_a^{comp}. The BSF was used to avoid an oscillatory position response due to the resonance. A stop-band was set to 300–500 Hz so that dominant resonant frequencies were included.

Two types of phase lag elements were considered, and the phase lag compensation was conducted inside the cutting force observer. First, the phase lag from the motor current command, I_a^{cmd}, to the actual output of the motor current, I_a^{res}, was considered. It was denoted as $H(s)$, and written as follows:

$$H(s) = \frac{\omega_{cc}}{s+\omega_{cc}} \cdot \frac{\omega_{comp}}{s+\omega_{comp}} \tag{8}$$

$H(s)$ was represented by two serially connected first-order LPFs. Although it was known that the bandwidth of the current control loop, ω_{cc} was designed to be 4000 rad/s, a phase delay adjuster was introduced to compensate for the actual phase delay from the dynamic characteristics of the motor. Thus, another first-order LPF, $\omega_{comp}/(s+\omega_{comp})$, was multiplied by $\omega_{cc}/(s+\omega_{cc})$ so that the accuracy of the dynamics between the motor current command, I_a^{cmd}, and the acceleration signals (a_t, $R\alpha_m$) could be enhanced as much as possible. The value of ω_{comp} was determined by swept excitation as discussed later. Second, the dead time, e^{-Ts}, during data acquisition was also considered. It was known that there were some dead time elements in our experimental setup. For example, a communication delay of 250 μs occurred while transferring the signal from the servo driver to the controller, and it took 60 μs to transform the signal at the DA board. Thus, it was preferable describe the available position and angle as $\hat{x}_t$ and $\hat{\theta}_m$. However, it was difficult to accurately identify all of the dead time elements from the equipment catalog values, and was more preferable to identify the actual phase lag. The amount of these two phase lags was identified experimentally, also by swept sine excitation. After this identification process, the phase lag between each control signal which was used in the estimation (i.e., I_a^{cmd}, $\hat{x}_t$, and $\hat{\theta}_m$) was set for the ideal condition by the phase lag compensation indicated in Fig. 9. For the swept sine excitation, a sinusoidally varying velocity command, whose frequency varied from 10 to 1000 Hz, was supplied. At that time, the position feedback loop was eliminated, to ensure stability while the DOB was in effect. I_a^{cmd}, $\hat{x}_t$, and $\hat{\theta}_m$ were acquired as time domain data from the control system. The acceleration signals $\hat{a}_t$ and $\hat{\alpha}_m$ were calculated from the backward difference of $\hat{x}_t$ and $\hat{\theta}_m$. By conducting fast Fourier transformation (FFT), two transfer functions, $\hat{a}_t/F_m$ and $R_n\hat{a}_m/F_m$, were experimentally identified, where $F_m(=K_{tn}I_a^{cmd}/R_n)$ was the motor thrust force command. Swept excitation results are shown in Figures 10 and 11 as solid blue lines. In addition, three calculated fitting curves from Eq. (5) are also presented in the figures. Curve fitting was conducted by following three steps. First, the mechanical parameters were determined by trial and error so that the anti-resonant frequency of $R_n\alpha_m/F_m$, and the resonant frequency of

Table 3 Parameters identified by swept sine excitation

J_r	Total inertia of motor, coupling, and ball screw [kg · m^2]	3.7×10^{-5}
M_t	Total movable mass [kg]	10.0
C_t	Viscous friction coefficient of translational element [N · s/m]	4.3×10^{3}
D_r	Viscous friction coefficient of rotational element [N · m · s/rad]	2.5×10^{-3}
K_r	Total rigidity of feed screw system [N/μm]	39.0
ω_{comp}	Cutoff frequency of compensation filter [rad/s]	6000.0
T_a, T_b	Dead time [ms]	0.7, 0.3
T_1, T_2, T_3	Dead time for phase lag compensation [ms]	0.7, 0.0, 0.4

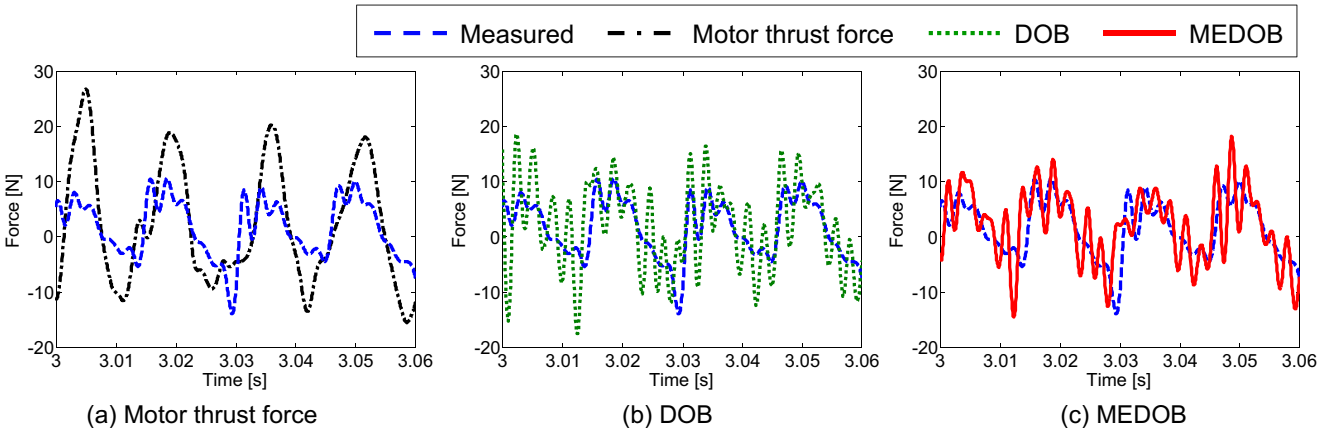

Fig. 12 Experimental results (spindle speed 2000 min^{-1})

a_t/F_m, would fit experimental results. Four resonance points are observed at 321, 355, 376, and 432 Hz in Fig. 11. Since the ball-screw-driven stage was modeled as a dual-inertia system, it was impossible to consider all of the resonant modes. In this study, a fitting curve was determined so as to capture the first two modes, which showed greater magnitudes. Second, the cutoff frequency, ω_{comp}, was determined so that the magnitude of the calculated result shown in Fig. 10a would fit that of the experimental results. Finally, the remaining phase lag was modeled by dead time elements so as to fit the calculated results to the experimental results. The identified dead times were $T_a = 0.7$ ms and $T_b = 0.3$ ms. As a result, the red dotted lines were obtained. After the phase lag compensation, the calculated results were in close agreement with the experimental results up to 400 Hz, monitoring the bandwidth of the cutting tests. Please note that there is the inevitable identification error in the higher frequency range, especially around 432 Hz, due to the use of the dual-inertia model.

The parameters identified by swept sine excitation are listed in Table 3. From the swept sine excitation results, it was found that $\hat{\theta}_m$ was the most-delayed signal of I_a^{cmd}, $\hat{x}_t$, and $\hat{\theta}_m$. Therefore, $\hat{\theta}_m$ was set as the standard of the lag compensation. T_1, T_2, and T_3 were determined so that all three signals were delayed 0.7 ms. The identified parameters shown in Table 3 were used as nominal values in the end milling tests.

5.3 Experimental results with phase lag compensation

For each cutting condition, cutting forces were estimated by three methods, the MEDOB, the DOB, and motor thrust force. Note that phase lag compensation was performed for all estimation methods for the sake of fair comparison. In addition, the friction force and torque were compensated for by the results of the idling test in time domain.

Figure 12 shows estimated cutting forces as time domain data for a spindle speed of 2000 min^{-1}. As seen from the figure, the cutting force was overestimated when monitoring only the motor thrust force. This occurred because the dynamics of the moving mass (i.e., inertia forces) were not considered in that method. Comparing the estimated cutting force from the DOB with that of the MEDOB, it was found that the former had a slightly noisier waveform. Figure 13 shows the FFT results for the cutting force from each method, using the same axis range for each graph. Although the height of the spectrum for the DOB and the MEDOB are close in value at 64 Hz, the higher harmonic components of the DOB were estimated as larger than those of the MEDOB and the measured cutting force. That suggested that the DOB was inferior to the MEDOB in estimating higher frequency components.

When the tooth-pass frequency of the cutting force was increased by setting the spindle speed to 7000 min^{-1}, another result was observed. As can be seen from Fig. 14a, not only was the force estimated by the motor thrust force overestimated, but also the temporal variations were unable to be captured. This happened because an extra frequency component, which resulted from runout in the spindle (at 119 Hz), was included, as shown in Fig. 15a. The values estimated using the DOB were also overestimated, as shown in Fig. 14b, which resulted from an estimation error of the tooth-pass frequency component as indicated in Fig. 15b.

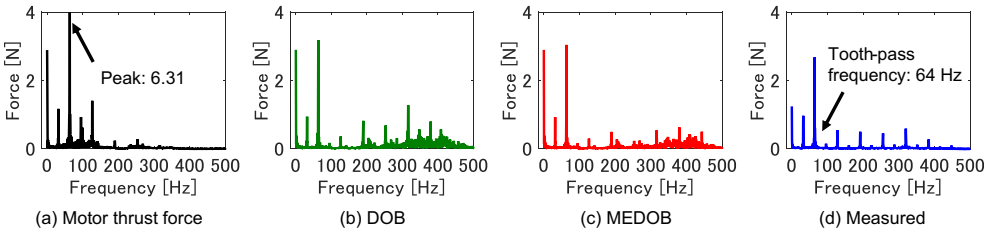

Fig. 13 FFT results of estimated and measured cutting forces (spindle speed 2000 min^{-1})

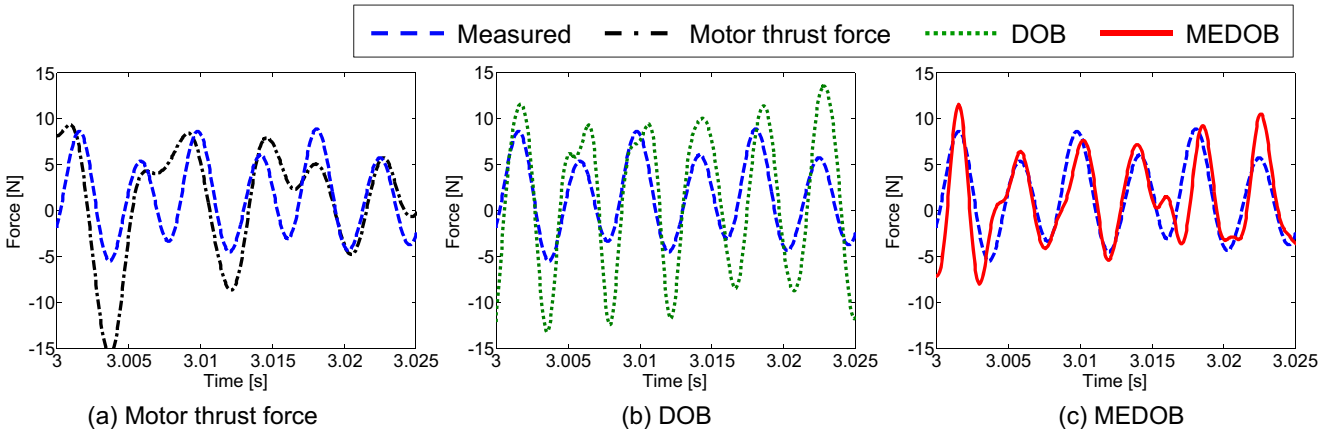

Fig. 14 Experimental results (spindle speed 7000 min^{-1})

On the other hand, the cutting force was estimated accurately with the use of the MEDOB.

Figures 16 and 17 show the results for a spindle speed of 10,000 min^{-1}. In this cutting condition, the tooth-pass frequency (337 Hz) of the cutting force came closest to the dominant resonant frequencies (321 and 355 Hz) of all the cutting conditions. As seen from Fig. 16a, b, the estimations using motor thrust force and the DOB were not valid. The motor current could not follow the high-frequency cutting force variations, and the amplitude of the motor thrust force was low. With regard to the DOB, the estimation was influenced by resonance, and the cutting force was overestimated. In contrast, the temporal variations of the cutting force were successfully monitored with high accuracy by using the MEDOB, even though its calculated frequency surpassed the bandwidth of the motor's current loop.

When the spindle speed was increased further to 12,000 min^{-1}, the cutting forces were overestimated even when the MEDOB was applied, as shown in Fig. 18. The tooth-pass frequency of the cutting force approached 400 Hz for this spindle speed. During the identification process for the mechanical parameters, higher resonance modes at 376 and 432 Hz were not considered. Thus, the identification error increased around 400 Hz, as shown in Fig. 11, which resulted in a reduction of the estimation accuracy. After arranging the sensors to monitor the dynamic behavior of each mechanical

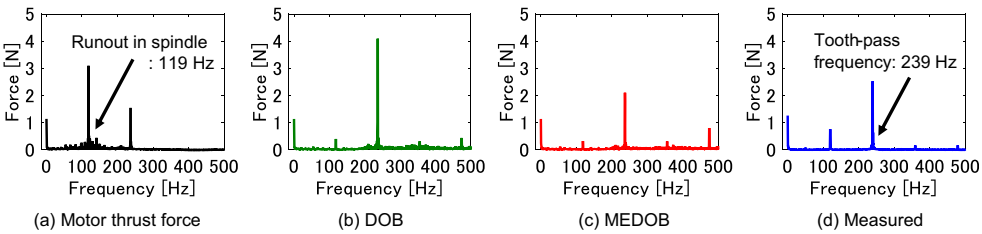

Fig. 15 FFT results of estimated and measured cutting forces (spindle speed 7000 min^{-1})

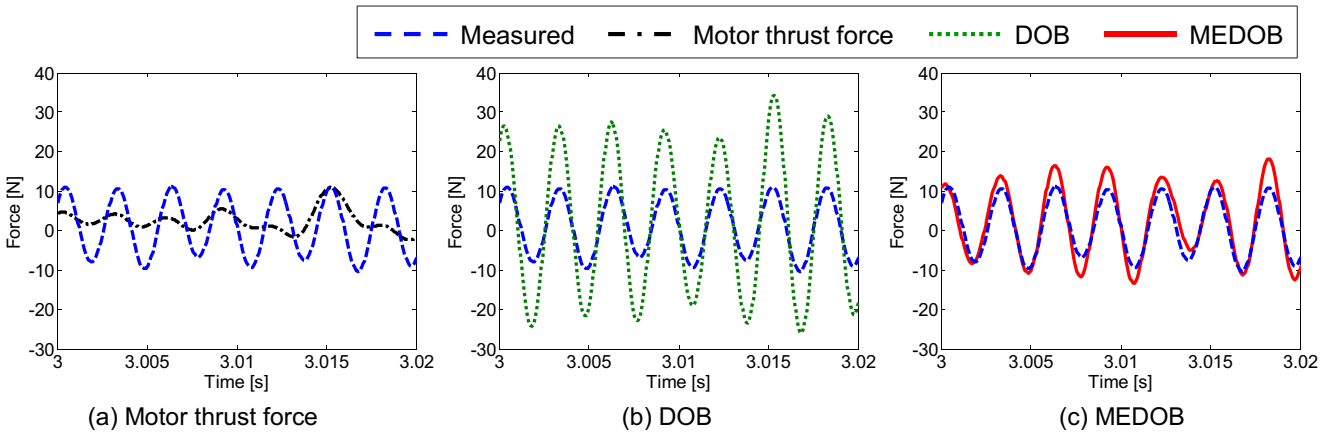

Fig. 16 Experimental results (spindle speed 10,000 min^{-1})

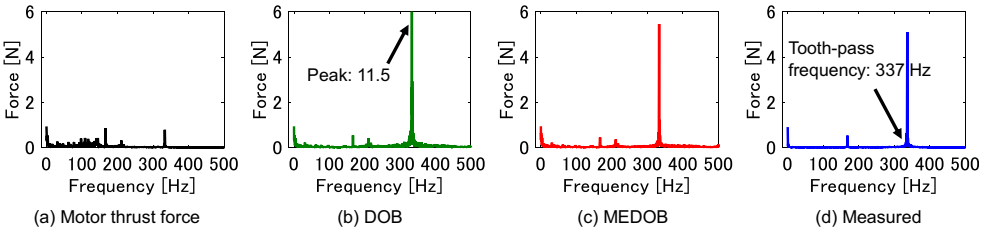

Fig. 17 FFT results of estimated and measured cutting forces (spindle speed 10,000 min^{-1})

element of the ball-screw-driven stage, the application of the multi-inertia model on behalf of the dual-inertia model was possible and lead to a more accurate cutting force estimation.

The standard deviation of the estimation error was also calculated, and the results are shown in Fig. 19. At lower spindle speeds, the discrepancy of the standard deviation between the DOB and the MEDOB was comparatively small, as depicted in Fig. 19a. However, the estimation accuracy falls for the DOB-based estimation at higher spindle speeds. With the use of the MEDOB, the standard deviation of the estimation errors was less than 5 N up to 10,000 min^{-1}, which is the range where the dual-inertia model was applicable. Validity of the phase lag compensation was also confirmed, and the results are shown in Fig. 19b. As seen from the figure, the phase lag compensation increased estimation accuracy up to 10,000 min^{-1}. Thus, it was confirmed that these were important in order to realize high precision and a wide band for cutting force estimation.

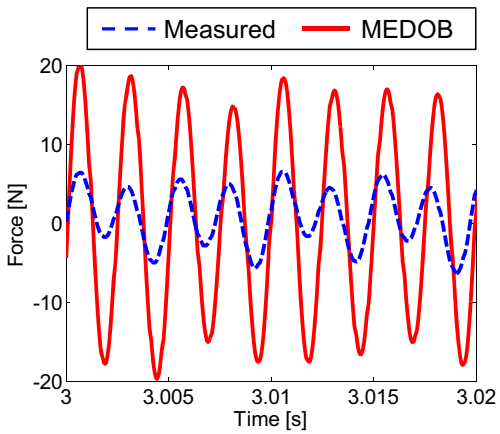

Fig. 18 Estimation results using MEDOB (spindle speed 12,000 min^{-1})

For further wideband cutting force estimation, two factors are worth consideration. First, to estimate the inertia forces more accurately, the accuracy of the velocity measurement should be increased. Since the velocity and acceleration signals are calculated from the position signals from the encoders, the accurate calculation of acceleration is difficult at higher frequencies. By increasing the resolution of the encoders, the accuracy of the velocity measurement would also be enhanced. Second, the application of the multi-inertia model would also be helpful to increase the modeling accuracy of the ball-screw-driven stage.

6 Conclusion

In this study, we developed a novel observer-based cutting force monitoring technology for full-closed controlled ball-screw-driven stages, which have been primarily employed in high-end machine tools in recent years. The feasibility of the proposed cutting force estimation method was experimentally evaluated by end milling tests. The following conclusions can be drawn from the study:

Considering that not only a rotary encoder but also a linear encoder was mounted to the full-closed controlled ball-screw-driven stage, a high-precision and wideband sensorless cutting force estimation method was proposed by applying a MEDOB. In this method, the cutting force was estimated by using three pieces of servo information: motor current command, motor angle, and displacement of the stage. The simulation results revealed that a cutting force estimation whose bandwidth exceeded the resonant frequency was theoretically possible with the use of the MEDOB. With the use of the conventional DOB in semi-closed controlled systems, it was

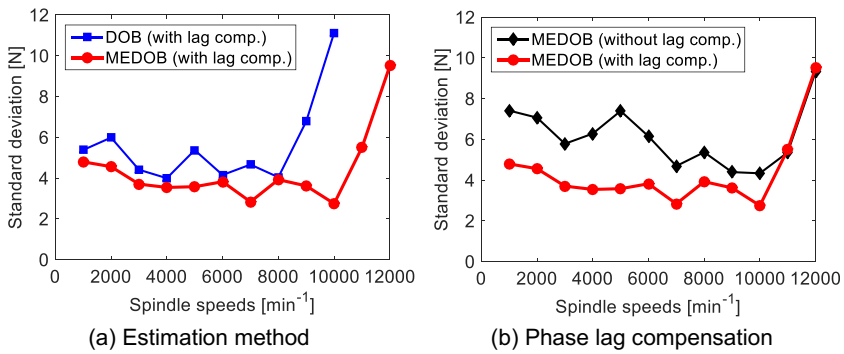

Fig. 19 Comparison of standard deviation of estimation errors

impossible to estimate the cutting force for a wider frequency range owing to the resonance of the driven system. A practical methodology was presented to apply the MEDOB to an actual ball-screw-driven stage as a wideband cutting force estimation method. The extra phase lags of the control signals that were used in the estimation were identified and compensated for by dead time and a low-pass filter. Consequently, it was found that the high-precision cutting force estimation whose bandwidth exceeded the current control loop was accomplished in actual end milling tests by the proposed method.

Acknowledgments This work was supported by JSPS KAKENHI, Grant No. 15H03904. The authors would like to express their deepest appreciation to Professor Kouhei Ohnishi for his comments and advice relating to this research.

References

1. Teti R, Jemielniak K, O'Donnell G, Dornfeld D (2010) Advanced monitoring of machining operations. CIRP Ann Manuf Technol 59: 717–739. doi:10.1016/j.cirp.2010.05.010
2. Denkena B, Mörke T, Krüger M et al (2014) Development and first applications of gentelligent components over their lifecycle. CIRP J Manuf Sci Technol 7:139–150. doi:10.1016/j.cirpj.2013.12.006
3. Shiraishi M (1988) Scope of in-process measurement, monitoring and control techniques in machining processes — part 1: in-process techniques for tools. Precis Eng 10:179–189. doi:10.1016/0141-6359(88)90052-9
4. Tönissen S, Koike R, Kakinuma Y et al (2014) Monitoring of tool collision in drilling by disturbance observer. CIRP J Manuf Sci Technol 7:274–282. doi:10.1016/j.cirpj.2014.05.004
5. Nouri M, Fussell BK, Ziniti BL, Linder E (2015) Real-time tool wear monitoring in milling using a cutting condition independent method. Int J Mach Tools Manuf 89:1–13. doi:10.1016/j.ijmachtools.2014.10.011
6. Altintas Y, Budak E (1995) Analytical prediction of stability lobes in milling. CIRP Ann Manuf Technol 44:357–362. doi:10.1016/S0007-8506(07)62342-7
7. Kakinuma Y, Sudo Y, Aoyama T (2011) Detection of chatter vibration in end milling applying disturbance observer. CIRP Ann Manuf Technol 60:109–112. doi:10.1016/j.cirp.2011.03.080
8. Cao H, Lei Y, He Z (2013) Chatter identification in end milling process using wavelet packets and Hilbert–Huang transform. Int J Mach Tools Manuf 69:11–19. doi:10.1016/j.ijmachtools.2013.02.007
9. Albrecht A, Park SS, Altintas Y, Pritschow G (2005) High frequency bandwidth cutting force measurement in milling using capacitance displacement sensors. Int J Mach Tools Manuf 45:993–1008. doi:10.1016/j.ijmachtools.2004.11.028
10. Albertelli P, Goletti M, Torta M et al (2016) Model-based broadband estimation of cutting forces and tool vibration in milling through in-process indirect multiple-sensors measurements. Int J Adv Manuf Technol 82:779–796. doi:10.1007/s00170-015-7402-x
11. Sarhan AAD, Matsubara A, Sugihara M et al (2006) Monitoring method of cutting force by using additional spindle sensors. JSME Int J Ser C 49:307–315. doi:10.1299/jsmec.49.307
12. Altintas Y (1992) Prediction of cutting forces and tool breakage in milling from feed drive current measurements. J Eng Ind 114:386–392. doi:10.1115/1.2900688
13. Lee JM, Choi DK, Kim J, Chu CN (1995) Real-time tool breakage monitoring for NC milling process. CIRP Ann Manuf Technol 44: 59–62. doi:10.1016/S0007-8506(07)62275-6
14. Jeong Y-H, Cho D-W (2002) Estimating cutting force from rotating and stationary feed motor currents on a milling machine. Int J Mach Tools Manuf 42:1559–1566. doi:10.1016/S0890-6955(02)00082-2
15. Sato R, Hasegawa M, Keiichi S (2013) Cutting force monitoring based on the frequency analysis of feed motor torques. J SME Jpn 2:7–12
16. Ohnishi K, Shibata M, Murakami T (1996) Motion control for advanced mechatronics. IEEE/ASME Trans Mechatron 1:56–67. doi:10.1109/3516.491410
17. Shinno H, Hashizume H, Yoshioka H (2003) Sensor-less monitoring of cutting force during ultraprecision machining. CIRP Ann Manuf Technol 52:303–306. doi:10.1016/S0007-8506(07)60589-7
18. Ibaraki S, Sakahira M, Saraie H et al (2004) On the monitoring of cutting forces in end milling processes: an estimation method by geometrically combining force vectors of servo motors and a spindle motor. J Japan Soc Precis Eng 70:1091–1095. doi:10.2493/jspe.70.1091 **(In Japanese)**
19. Takei M, Kurihara D, Katsura S, Kakinuma Y (2011) Hybrid control for machine tool table applying sensorless cutting force monitoring. Int J Autom Technol 5:587–593
20. Mitsantisuk C, Nandayapa M, Ohishi K, Katsura S (2013) Design for sensorless force control of flexible robot by using resonance ratio control based on coefficient diagram method. Autom J Control Meas Electron Comput Commun 54:62–73. doi:10.7305/automatika.54-1.311
21. Yuki K, Murakami T, Ohnishi K (1993) Vibration control of 2 mass resonant system by resonance ratio control. Proc. IECON'93 - 19th Annu. Conf. IEEE Ind. Electron. IEEE, pp 2009–2014
22. Matsubara A (2008) Design and control of precision positioning and feed drive systems. Morikita Publishing Co. Ltd, Japan **(In Japanese)**
23. Koike R, Kakinuma Y, Aoyama T (2014) Drill fracture detection by integrating disturbance observer and rotational digital filter. CIRP J Manuf Sci Technol 7:177–184. doi:10.1016/j.cirpj.2014.04.001
24. Altintas Y (2012) Manufacturing automation: metal cutting mechanics, machine tool vibrations, and CNC design. Cambridge University Press, Cambridge
25. Ro PI, Shim W, Jeong S (2000) Robust friction compensation for submicrometer positioning and tracking for a ball-screw-driven slide system. Precis Eng 24:160–173. doi:10.1016/S0141-6359(00)00030-1
26. Fukada S, Fang B, Shigeno A (2011) Experimental analysis and simulation of nonlinear microscopic behavior of ball screw mechanism for ultra-precision positioning. Precis Eng 35:650–668. doi:10.1016/j.precisioneng.2011.05.006
27. Itagaki H, Tsutsumi M (2014) Control system design of a linear motor feed drive system using virtual friction. Precis Eng 38:237–248. doi:10.1016/j.precisioneng.2013.09.002